

Multi-epoch X/UV variability in the CDF-S

AGN10, 2012 September 10-13, Roma

Antonucci, Vagnetti, Trevese,
and XMM CDF-S Team

Context

Present analysis is part of a study about the variability of the X-ray-to-optical ratio of AGNs based on simultaneous X/UV measurements.

1. **XMMSSC/XMMOMSUSS data** [Vagnetti *et al.* 2010]
dispersion in the $\alpha_{ox} - L_{UV}$ relation and intrinsic variability of the X-ray/UV ratio
2. **Grupe *et al.* 2010 *Swift* catalogue** (in progress, poster)
analysis of a low-redshift sample and possible contamination due to host galaxy optical emission
3. **XMM Deep Survey in the CDF-S**
individual pattern of the sources in the $\alpha_{ox} - L_{UV}$ plane, light-curves and structure functions

XMM Deep Survey in the CDF-S [Comastri *et al.* 2011]:

- observations performed in four different epochs (July 2008-February 2010), with archival data obtained in the period July 2001-January 2002
- total exposures of about 2.82Ms for the two MOS detectors and 2.45Ms for the *pn* camera
- the survey encompasses the CDF-S and most of its flanking fields (E-CDF-S)

X-ray/UV ratio of AGNs

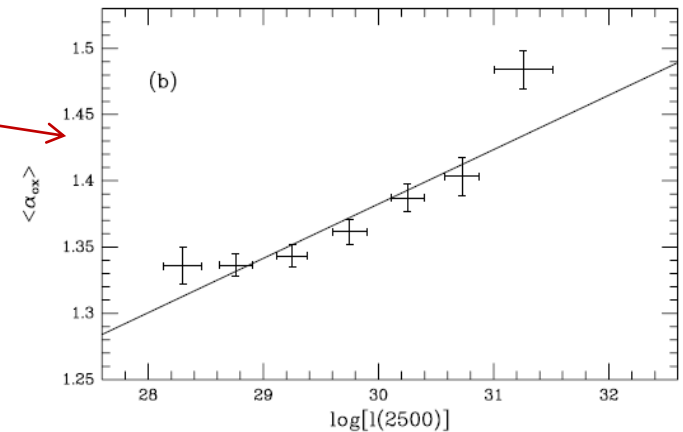
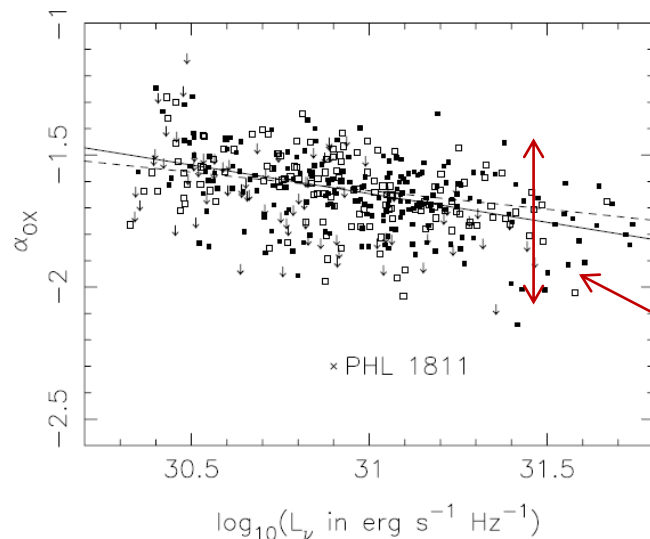
$\alpha_{ox} - L_{UV}$ relation:

- energy generation mechanisms and accretion processes in the AGNs
- $L_X \propto L_{UV}^\gamma$, $0.5 \leq \gamma \leq 0.8$; $L_X - L_{UV}$ relation depends on the structural parameters of the disk-corona coupling: covering factor, optical depth of the coronal gas... [Haardt & Maraschi 1991, 1993]

$$\alpha_{ox} = \frac{\log(L_{2keV} / L_{250nm})}{\log(\nu_{2keV} / \nu_{250nm})} = 0.3838 \left(\frac{L_{2keV}}{L_{250nm}} \right)$$

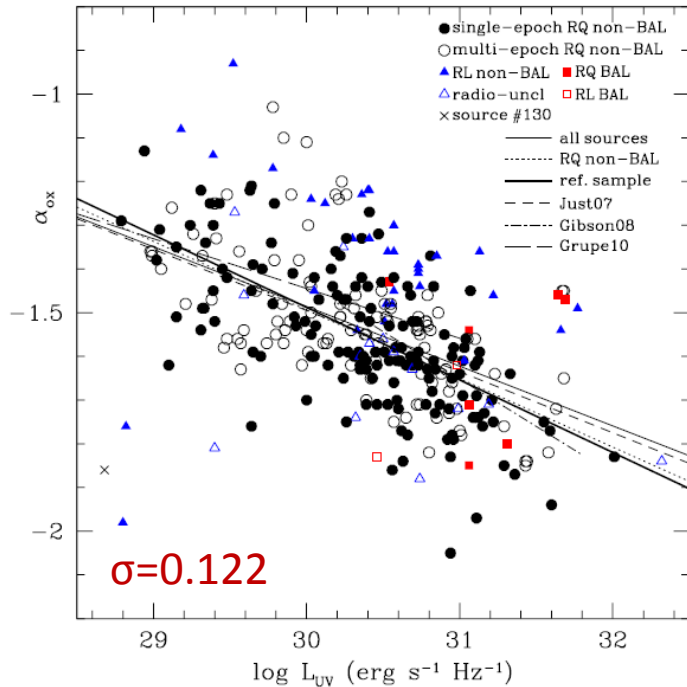
$$\alpha_{ox} = a \cdot \log L_{UV} + const$$

probably non-linear relation [Anderson *et al.* 2003]

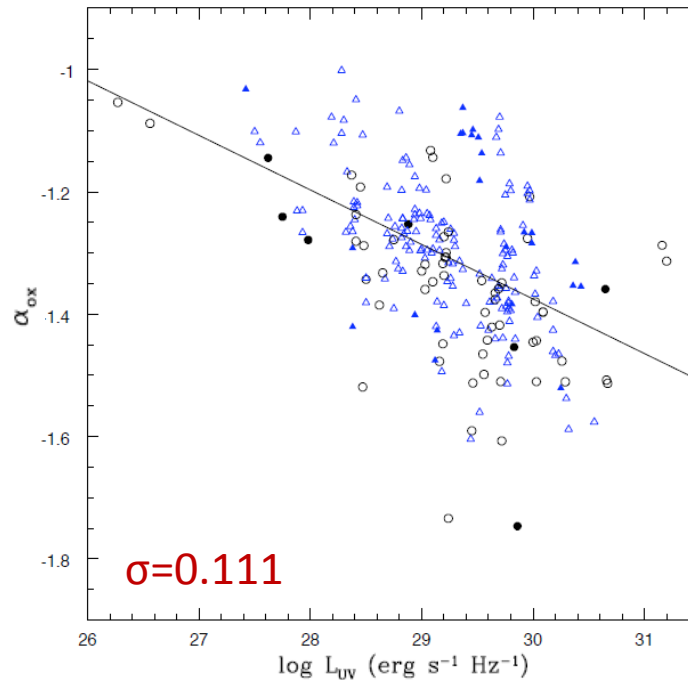


great dispersion with respect to mean relation, possibly due to variability and/or non-simultaneity of X and UV measurements [Gibson *et al.* 2008]

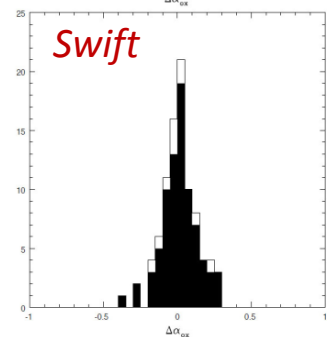
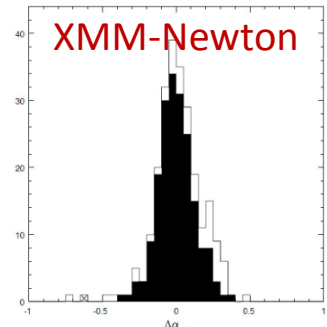
Dispersion with simultaneous X/UV data



XMM serendipitous surveys



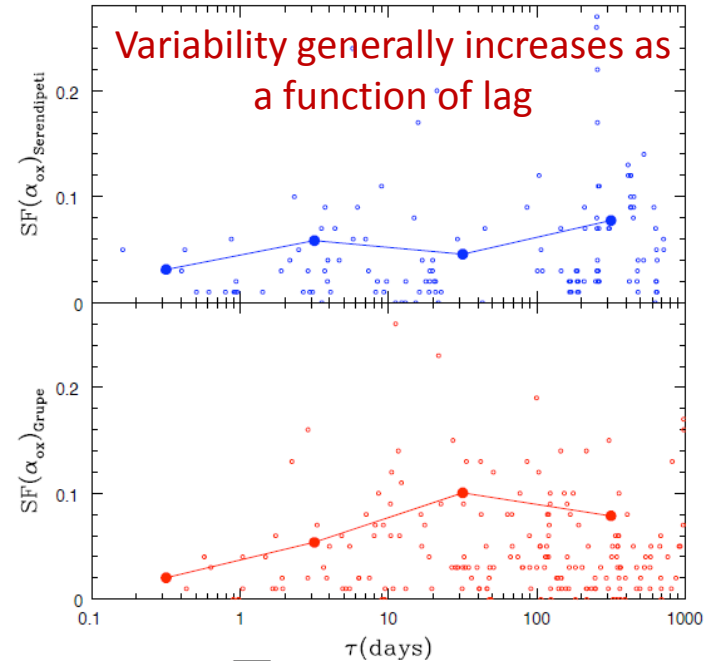
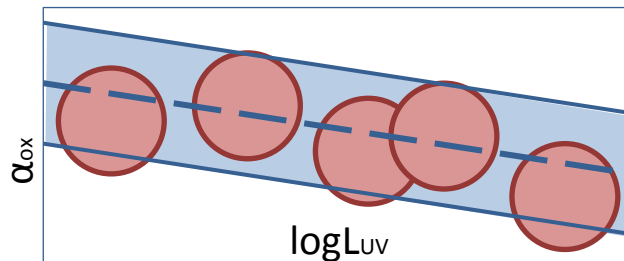
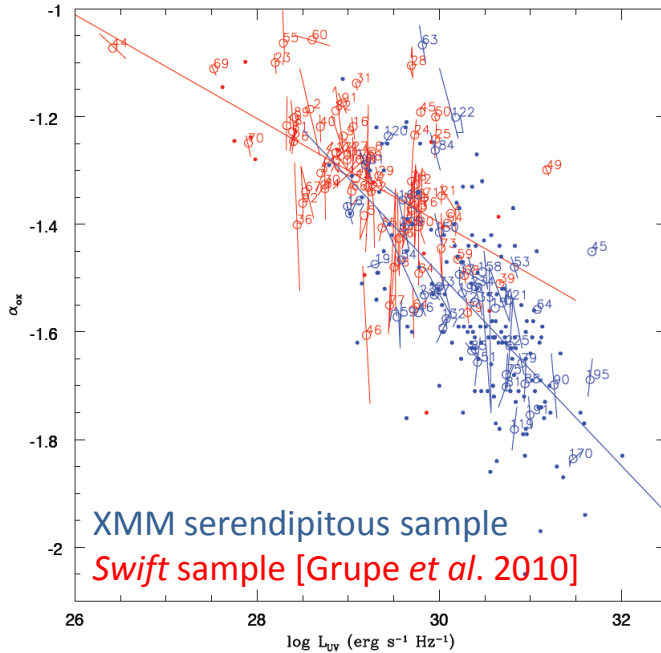
Swift sample [Grupe *et al.* 2010]



Artificial variability (non-simultaneity) has marginal effects on the scatter ($0.10 \leq \sigma \leq 0.14$, [Just *et al.* 2007, Gibson *et al.* 2008])

- intra-source dispersion: intrinsic α_{ox} variations for individual sources
- inter-source dispersion: intrinsic differences in the average α_{ox} values from source to source, perhaps related to dissimilar conditions in the emitting regions

Intra-source and inter-source dispersion



$$SF(\tau) = \sqrt{\frac{\pi}{2}} \langle |\alpha_{ox}(t + \tau) - \alpha_{ox}(t)| \rangle$$

$$\sigma_{tot}^2 = \sigma_{intra-source}^2 + \sigma_{inter-source}^2$$

$$\sigma_{intra-source}^2 \geq 0.3\sigma_{tot}^2$$

- Intra-source dispersion accounts for a considerable part of the total variance, and its contribution is comparable to the inter-source scatter.
- The dispersion introduced by variability is mostly caused by the intermediate and long timescale variations, which are expected to be driven by the optical variability.

XMM Deep Survey in the CDF-S

Exposures (ks)

n	Obsid	Time	X-ray	UVW2	UVM2	UVW1	U	B	V
1	0108060401	2001.5681	49	19	8				
2	0108060501	2001.5698	64	20	8	8	4	4	
3	0108060601	2002.0344	65	15	5	5	5	3	
4	0108060701	2002.0376	94	20	10	10	5	5	
5	0108061801	2002.0430	63	12	5	5	2	2	
6	0108061901	2002.0457	54	10	5	5	2	2	
7	0108062101	2002.0540	62	9	8	5	2	2	
8	0108062301	2002.0603	88	5	5	5	2	2	
9	0555780101	2008.5088	133		31	44	44		
10	0555780201	2008.5142	133		32	44	44		
11	0555780301	2008.5200	123		31	42	37		
12	0555780401	2008.5255	122		30	40	39		
13	0555780501	2009.0160	113	24	16	4	4	8	4
14	0555780601	2009.0268	118	30	12	4	4	8	8
15	0555780701	2009.0323	118	34	12	4	4	8	4
16	0555780801	2009.0431	120	36	10	4	4	8	8
17	0555780901	2009.0486	121	31	12	4	4	8	8
18	0555781001	2009.0596	125	34	12	3	4	7	7
19	0555782301	2009.0651	125	34	12	3	3	7	4
20	0604960301	2009.5077	122	19		50	38		
21	0604960201	2009.5406	121	23		36	50		
22	0604960101	2009.5675	129	21		50	50		
23	0604960401	2009.5730	133	16		35	50		
24	0604961101	2010.0103	120	7		50	50		
25	0604961201	2010.0213	120	32		25	50		
26	0604960701	2010.0322	120	7		50	50		
27	0604960501	2010.0486	46				40		
28	0604961301	2010.0519	21			13	5		
29	0604960601	2010.0705	125	23		50	40		
30	0604960801	2010.0978	121	21		40	45		
31	0604960901	2010.1142	125			10	92		
32	0604961001	2010.1196	122	21		45	36		
33	0604961801	2010.1305	125	22		45	45		

8 observations
period 2001-2002
(PI: Bergeron)

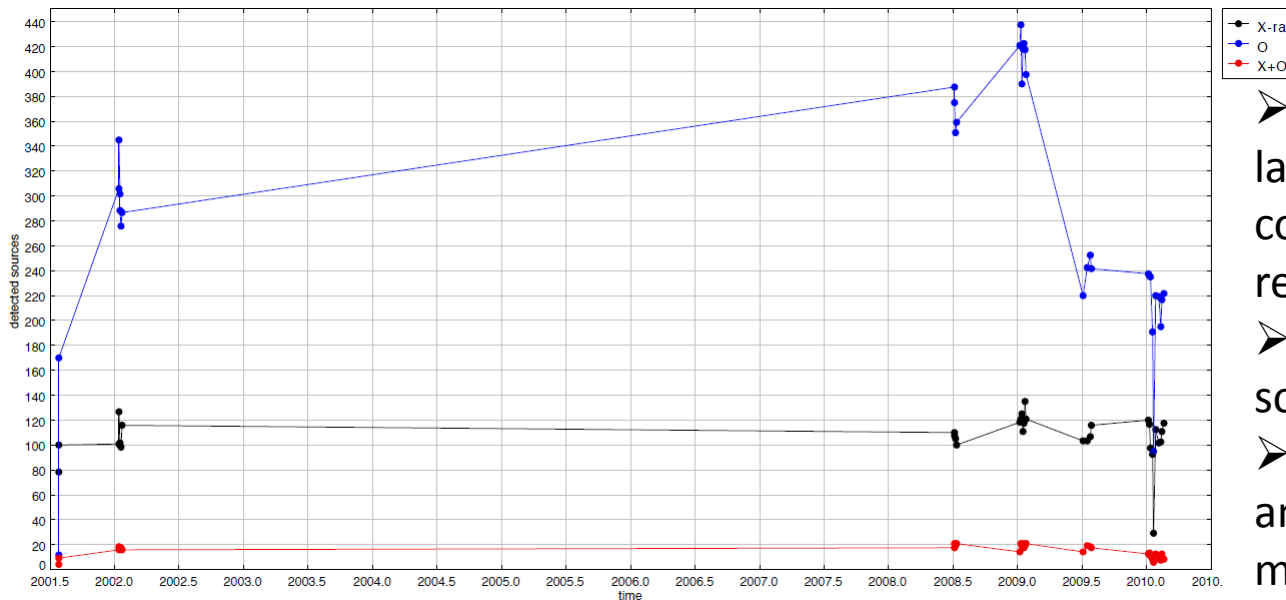
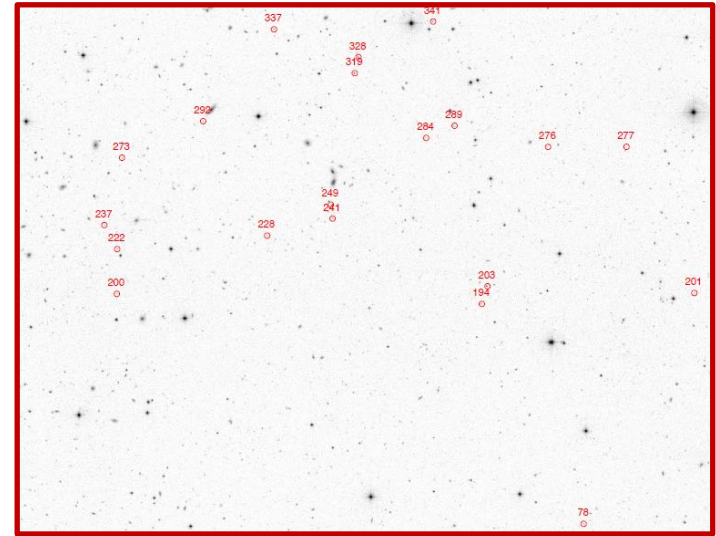
- shorter X-ray and optical
exposures

25 observations
period 2008-2010
(PI: Comastri)

- typical X-ray exposure of
about 120ks
- heterogeneous use of the
optical/UV filters (OM
exposures mainly in the U and
UVW1)

CDF-S sample: identifications

- Correlation of X-ray and optical/UV data tables (from the Heasarc Archive) with a joint reference catalogue of redshifts for each epoch
- Match of X-ray/z and UV/z tables obtained in the previous step
- Joining of X-ray/UV/z matches achieved for all the observations



- Optical identifications largely are lacking in X-ray counterpart, being represented by galaxies
- Most of the X-ray sources are AGNs
- Few objects have X-ray and UV simultaneous measurements, up to 20 for epoch

CDF-S sample

65 sources with X-ray and UV simultaneous measurements:
 20 multi-epoch AGNs, 13 mono-epoch AGNs, 32 galaxies
 and unclassified objects

Optical coordinates from
 redshift catalogues

X-ray coordinates from stacked
 catalogue [Ranalli *et al.*, in progress]

n	z	ep	O-class	X-class	Optical coordinates from redshift catalogues		X-ray coordinates from stacked catalogue [Ranalli <i>et al.</i> , in progress]	
					RAJ2000	DEJ2000	RA	DEC
78	0.737	2	HEX	AGN-2	52.98075	-27.91344	52.98066	-27.91376
194	2.81	7	BLAGN	QSO-2	53.03942	-27.80189	53.03947	-27.80215
200	2.579	25	BLAGN	QSO-1	53.24929	-27.79672	53.24949	-27.79664
201	2.709	6	UAGN		52.91729	-27.79619	52.91637	-27.79593
203	0.543	33	BLAGN	QSO-1	53.03617	-27.79289	53.03594	-27.79297
222	0.424	5	LEX	AGN-2	53.24904	-27.774	53.24856	-27.77401
228	1.216	21	BLAGN	AGN-1	53.16287	-27.76722	53.16338	-27.76793
237	0.619	6	BLAGN	AGN-1	53.25642	-27.76183	53.25673	-27.76214
241	1.209	29	BLAGN	QSO-1	53.12525	-27.75853	53.12479	-27.75832
249	0.738	26	BLAGN	AGN-1	53.12625	-27.7515	53.1255	-27.75104
273	0.733	12	BLAGN	AGN-1	53.24621	-27.72764	53.24595	-27.72779
276	1.037	17	BLAGN	AGN-1	53.00146	-27.72211	53.00248	-27.72286
277	1.318	2	UAGN		52.95637	-27.72203	52.95618	-27.72149
284	0.569	8	BLAGN	AGN-1	53.07146	-27.71761	53.07126	-27.71773
289	0.605	30	LEX	AGN-2	53.05517	-27.71142	53.05594	-27.71188
292	0.979	12	LEX	QSO-1	53.19958	-27.70911	53.20021	-27.70915
319	0.734	32	BLAGN	QSO-1	53.1125	-27.68475	53.11234	-27.68497
328	1.031	30	BLAGN	QSO-1	53.11037	-27.67658	53.11019	-27.67662
337	0.837	31	BLAGN	QSO-1	53.15888	-27.6625	53.15889	-27.66236
341	1.324	4	BLAGN	QSO-1	53.0675	-27.6585	53.06758	-27.65818

BLAGN: objects with emission lines broader than 2000km/s
 HEX: sources with unresolved emission lines and exhibiting high ionization lines (AGN activity)
 LEX: objects with unresolved emission lines consistent with a HII region-type spectra
 UAGN: unobscured AGN

QSO-1: $\log L(0.5-10\text{keV}) \geq 44$, $\text{HR} \leq -0.2$
 AGN-1: $42 \leq \log L(0.5-10\text{keV}) \leq 44$, $\text{HR} \leq -0.2$
 QSO-2: $\log L(0.5-10\text{keV}) \geq 44$, $\text{HR} > -0.2$
 AGN-2: $41 \leq \log L(0.5-10\text{keV}) \leq 44$, $\text{HR} > -0.2$
 [Szkoly *et al.* 2004, Treister *et al.* 2008]

CDF-S sample: evaluation of the monochromatic luminosities

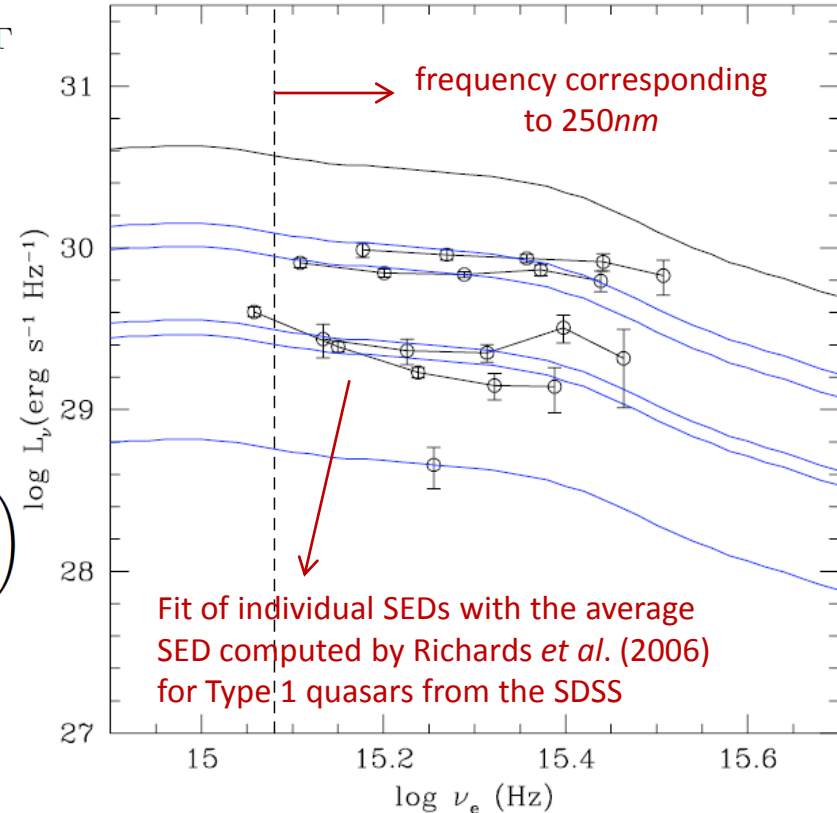
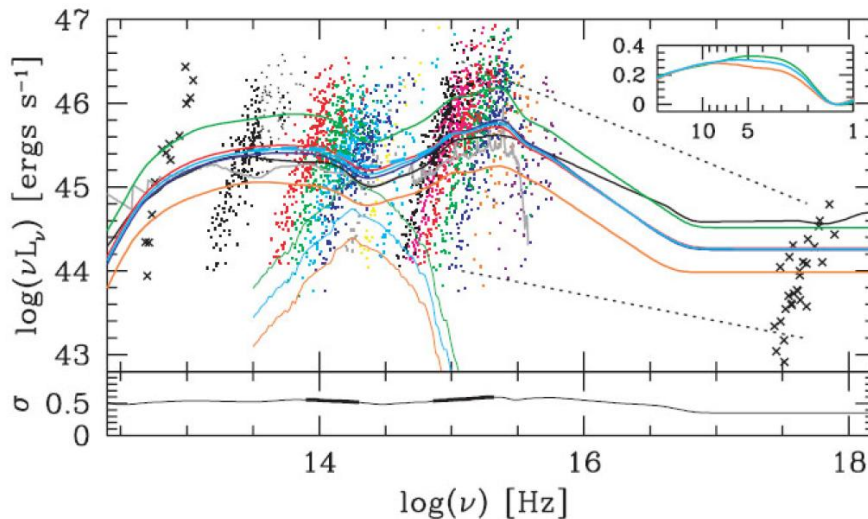
$$F_X(2 - 4.5\text{keV}) = \int_{2\text{keV}}^{4.5\text{keV}} F_\nu(2\text{keV}) \left(\frac{\nu}{\nu_{2\text{keV}}} \right)^{1-\Gamma}$$

$$F_\nu(2\text{keV}) = \frac{F_X(2 - 4.5\text{keV})}{\nu_{2\text{keV}}} \cdot \frac{2 - \Gamma}{2.25^{2-\Gamma} - 1}$$

$$L_\nu(2\text{keV}) = F_\nu(2\text{keV}) \cdot \frac{4\pi D_L^2}{(1+z)^{2-\Gamma}}$$

$$L_\nu(\nu_e) = F_\nu(\nu_o) \cdot \frac{4\pi D_L^2}{1+z}$$

$$\alpha_{ox} = \frac{\log(L_{2\text{keV}}/L_{250\text{nm}})}{\log(\nu_{2\text{keV}}/\nu_{250\text{nm}})} = 0.3838 \left(\frac{L_{2\text{keV}}}{L_{250\text{nm}}} \right)$$



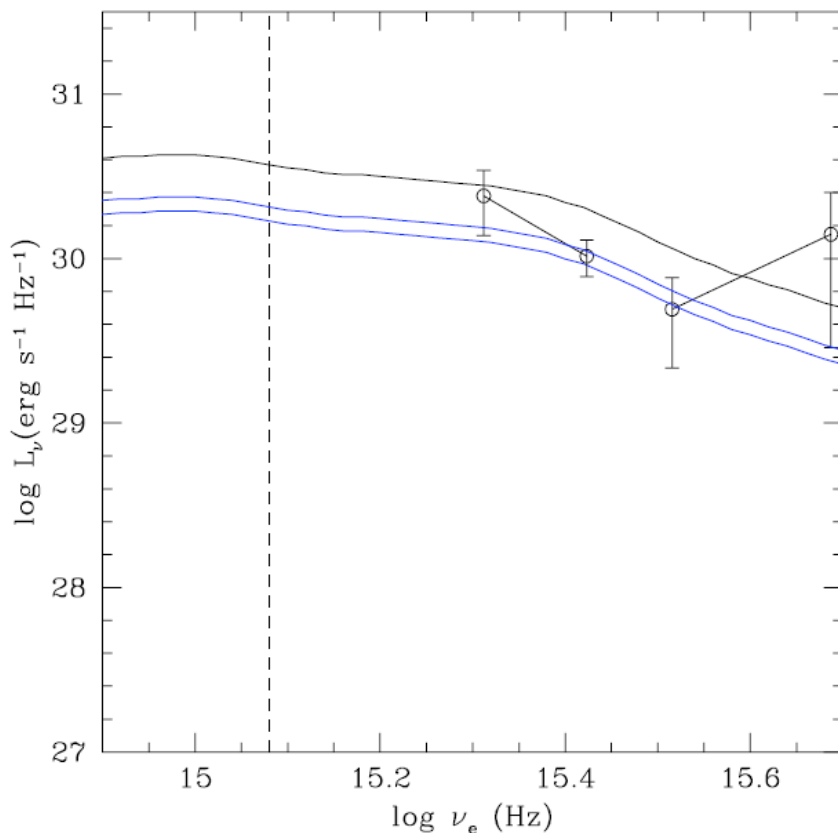
$$\chi^2 = \sum_{i=1}^N \left[\frac{y_i - a \cdot X(x_i)}{\sigma_i} \right]^2$$

$$a = \frac{\sum_{i=1}^N \frac{y_i \cdot X(x_i)}{\sigma_i^2}}{\sum_{i=1}^N \frac{[X(x_i)]^2}{\sigma_i^2}}$$

CDF-S sample: evaluation of the monochromatic luminosities

The evaluation of monochromatic UV luminosity carried out as an interpolation with the Richards function offers some advantages:

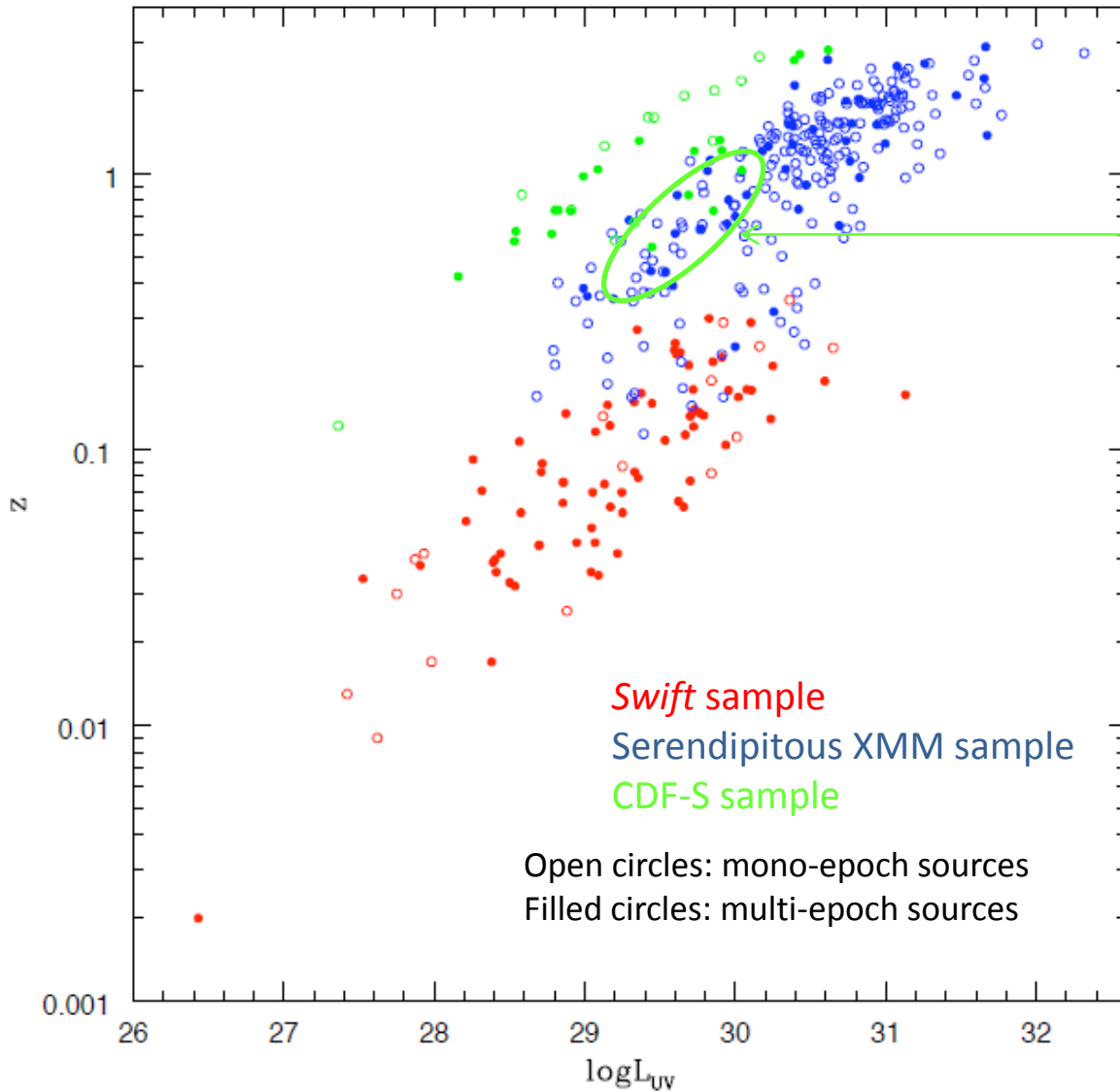
- straight extrapolation from the two lowest frequency points could yield unrealistic estimates of the luminosity, because of the inclination of that part of the SED;
- all the available data are considered, differently than the extrapolation from the lowest frequency point;
- this method allows to consider the errors and to assign suitable weights to the SED points.



To fit a set of data to a model which is not just a linear combination, but an arbitrary function of x (*basis function*), it is possible to calculate the value of the parameter " a " that minimize the merit function χ [Press *et al.* 1986]. In this case, X corresponds to the Richards function, while the ordinates represent the values of luminosity of a certain source obtained with different filters.

$$\chi^2 = \sum_{i=1}^N \left[\frac{y_i - a \cdot X(x_i)}{\sigma_i} \right]^2$$
$$a = \frac{\sum_{i=1}^N \frac{y_i \cdot X(x_i)}{\sigma_i^2}}{\sum_{i=1}^N \frac{[X(x_i)]^2}{\sigma_i^2}}$$

Samples in the luminosity-redshift plane

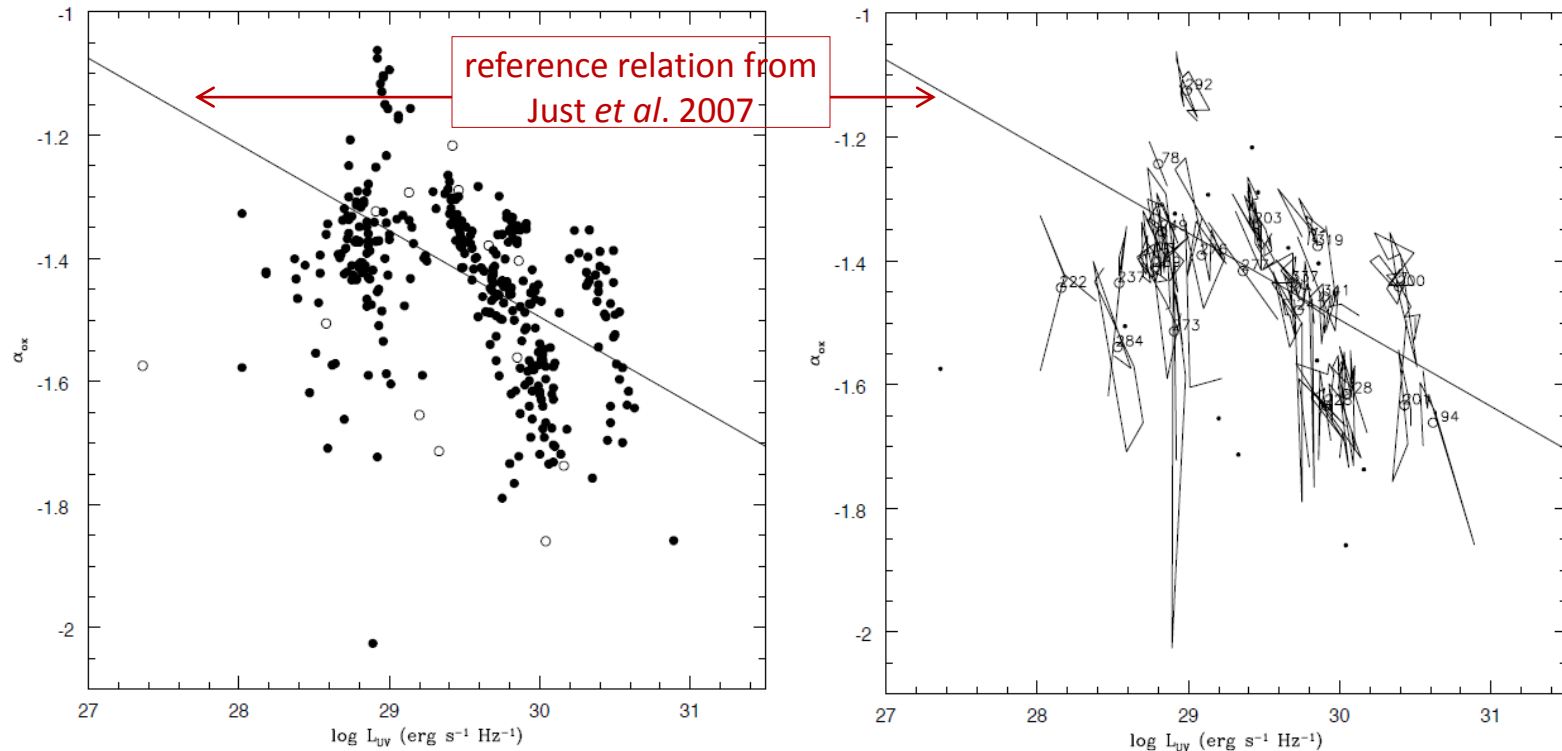


relatively brighter
sources

Faint objects dominate the CDF-S
sample.

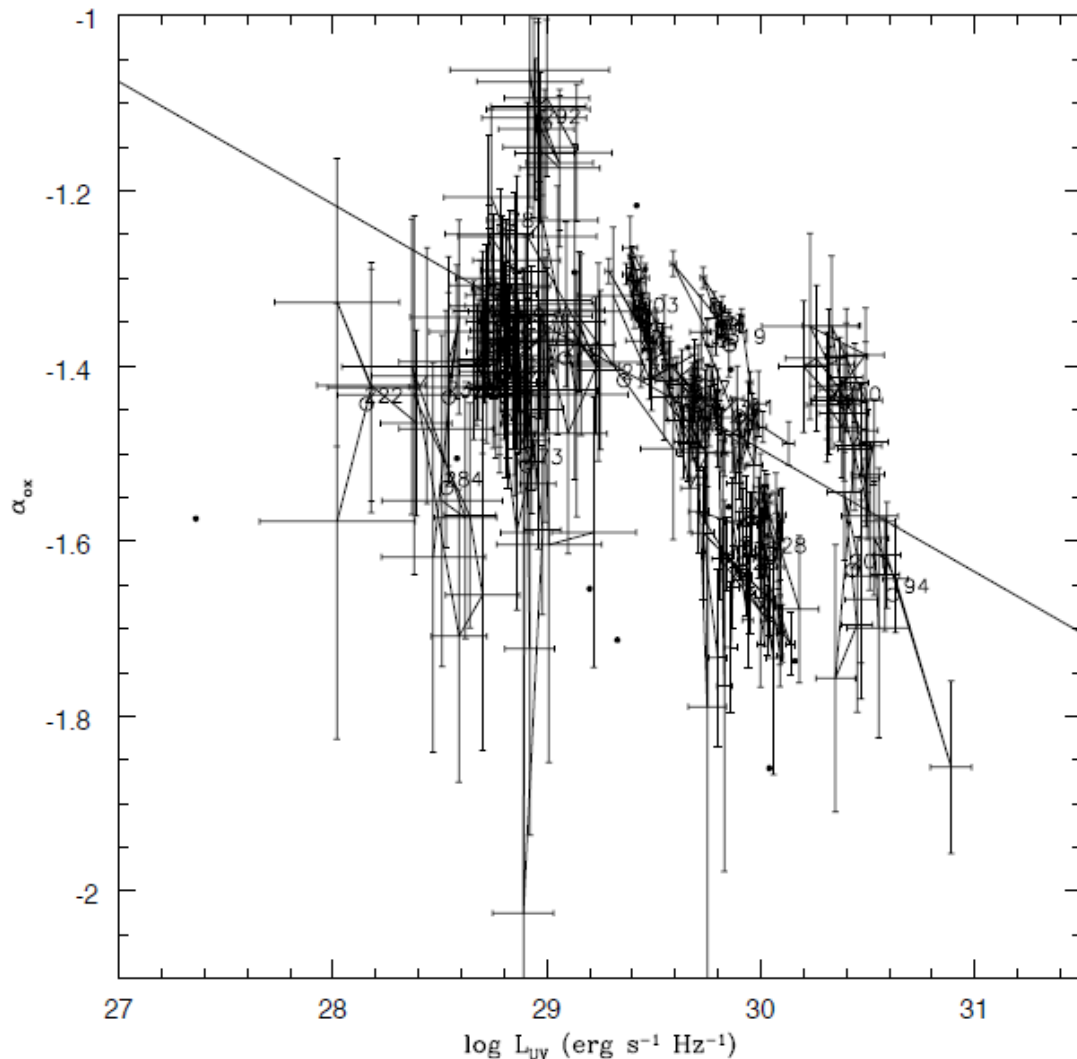
Underlined sources have the best
S/N ratio, allowing the subtraction
of photometric noise.

CDF-S sample: $\alpha_{ox} - L_{UV}$ relation and intra-source dispersion



CDF-S sample provide detailed information about individual variability. The samples analysed in the previous works generally have 2-3 observations for multi-epochs sources, while in this case some sources have more than 20 simultaneous X/UV measurements.

CDF-S sample: intra-source dispersion and errors



SSCs	mean	min	max
$\delta\alpha_{\text{ox}}$	0.043	0.002	0.282
$\delta\log L_X$	0.066	0.003	0.548
$\delta\log L_{\text{UV}}$	0.047	0.002	0.228

<i>Swift</i>	mean	min	max
$\delta\alpha_{\text{ox}}$	0.008	<0.001	0.026
$\delta\log L_X$	0.019	<0.001	0.066
$\delta\log L_{\text{UV}}$	<0.001	<0.001	0.003

CDF-S	mean	min	max
$\delta\alpha_{\text{ox}}$	0.063	0.009	0.737
$\delta\log L_X$	0.084	0.013	1.779
$\delta\log L_{\text{UV}}$	0.079	0.009	0.372

Detailed information about individual variability, but in presence of great errors.

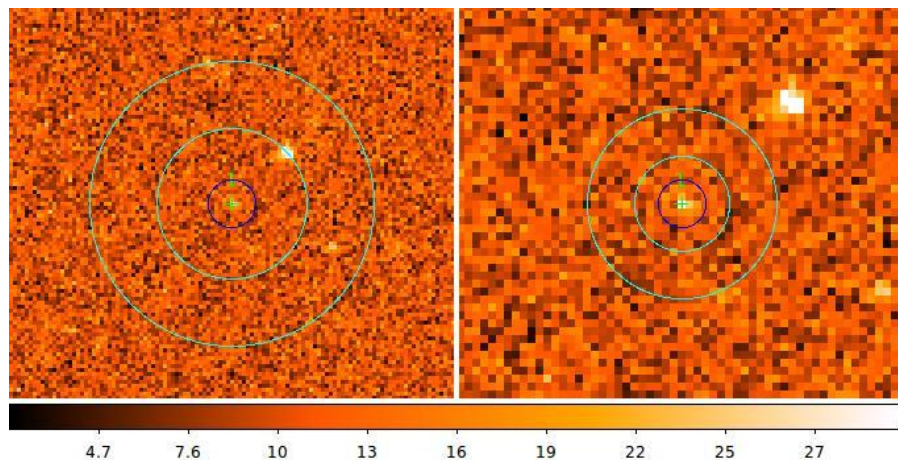
CDF-S sample: intra-source dispersion and errors

Photometric noise dominates intrinsic variability in the total sample ensemble structure function.

Possible improvements:

- get optimised X-ray fluxes (from the collaboration, in progress);
- compute the optical fluxes increasing S/N ratio (through the interactive photometric analysis of the OM images with SAS).

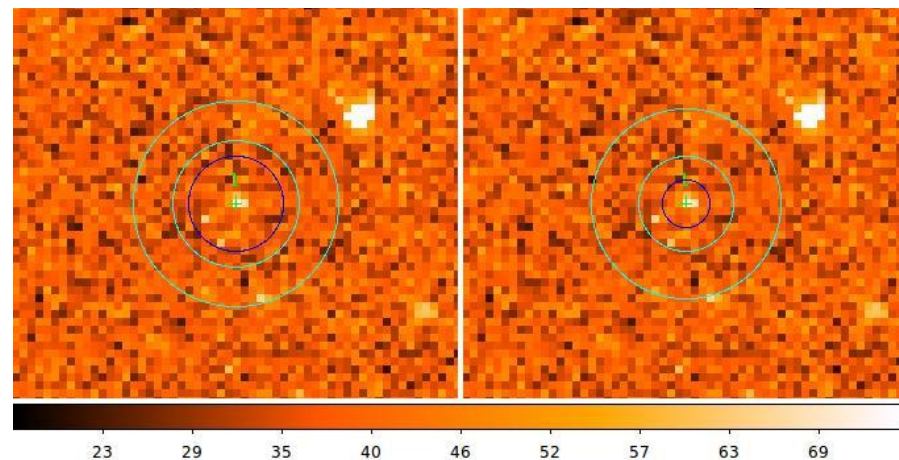
source 276, epoch 3, filter UVW1



S/N=2.36, $m=21.10\pm0.47$

S/N=4.11, $m=21.02\pm0.43$

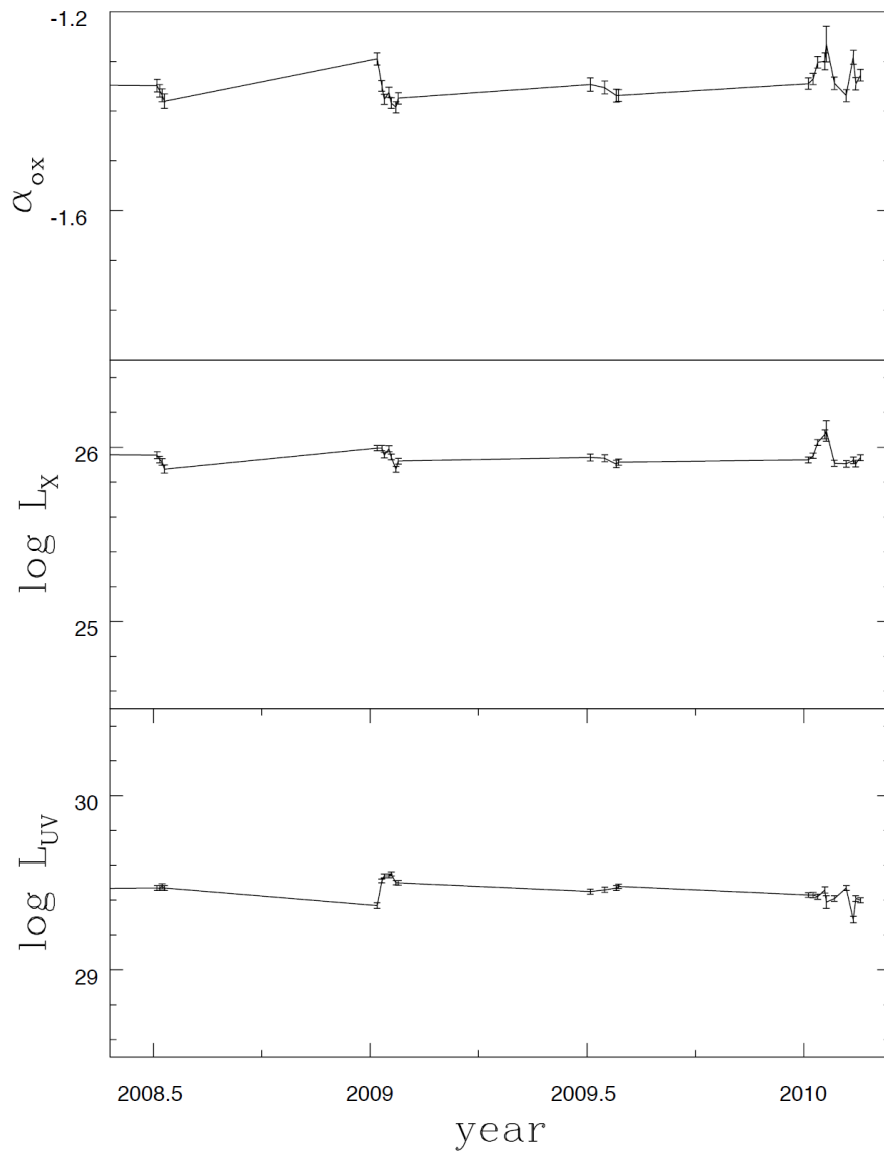
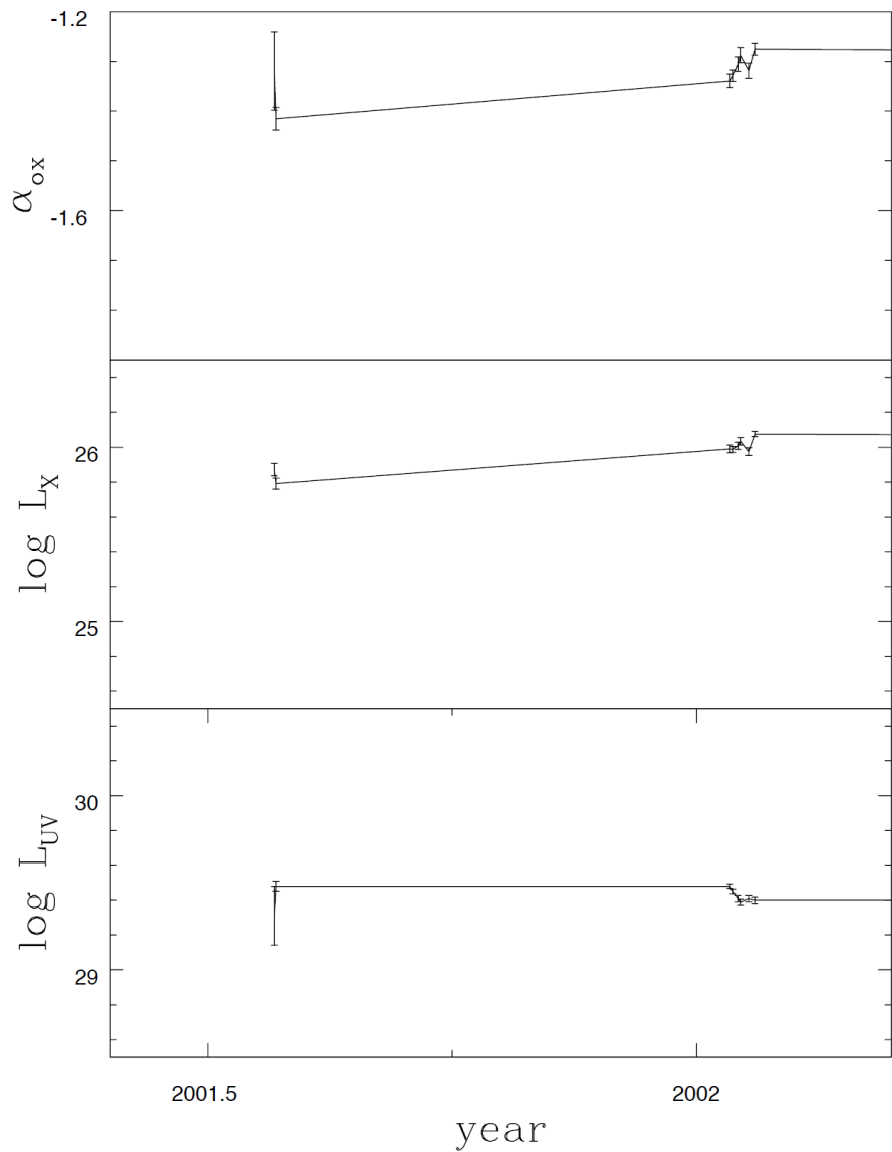
source 276, epoch 24, filter U



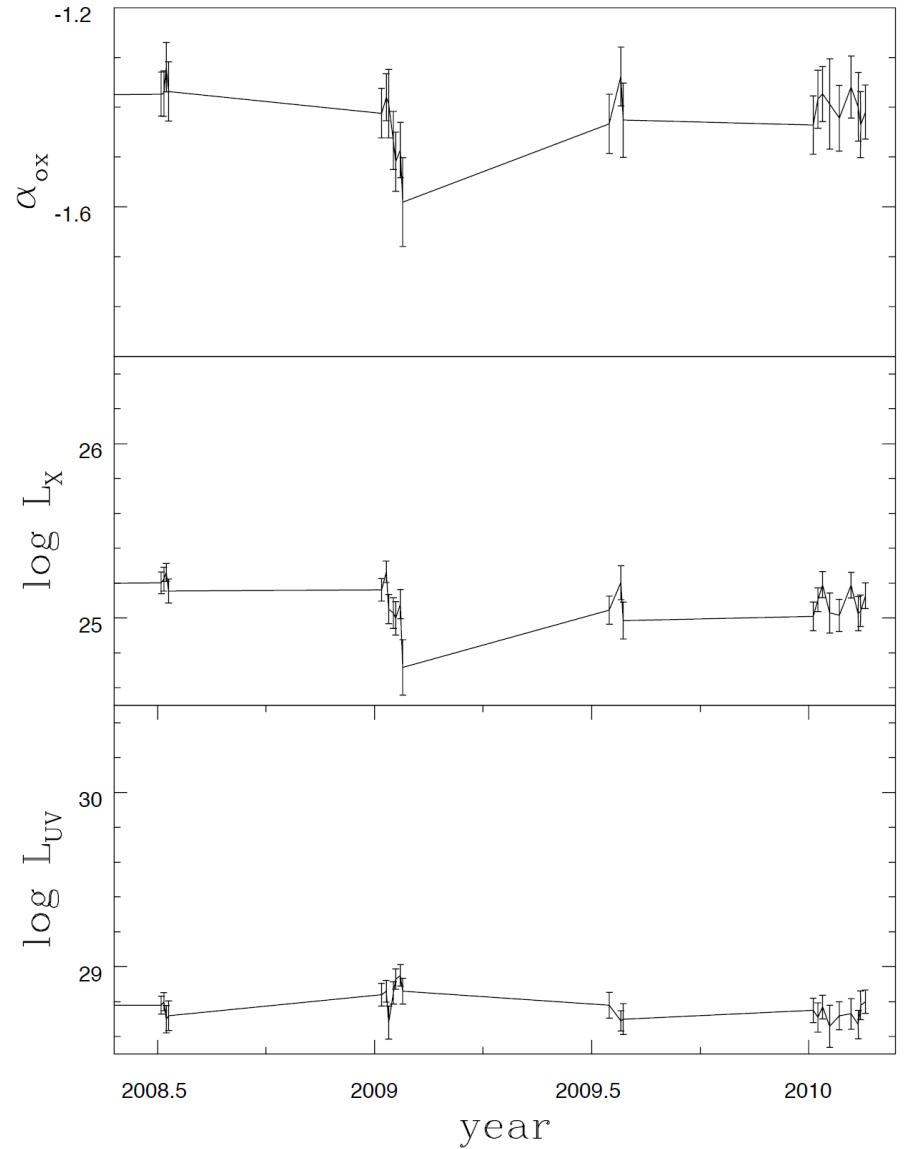
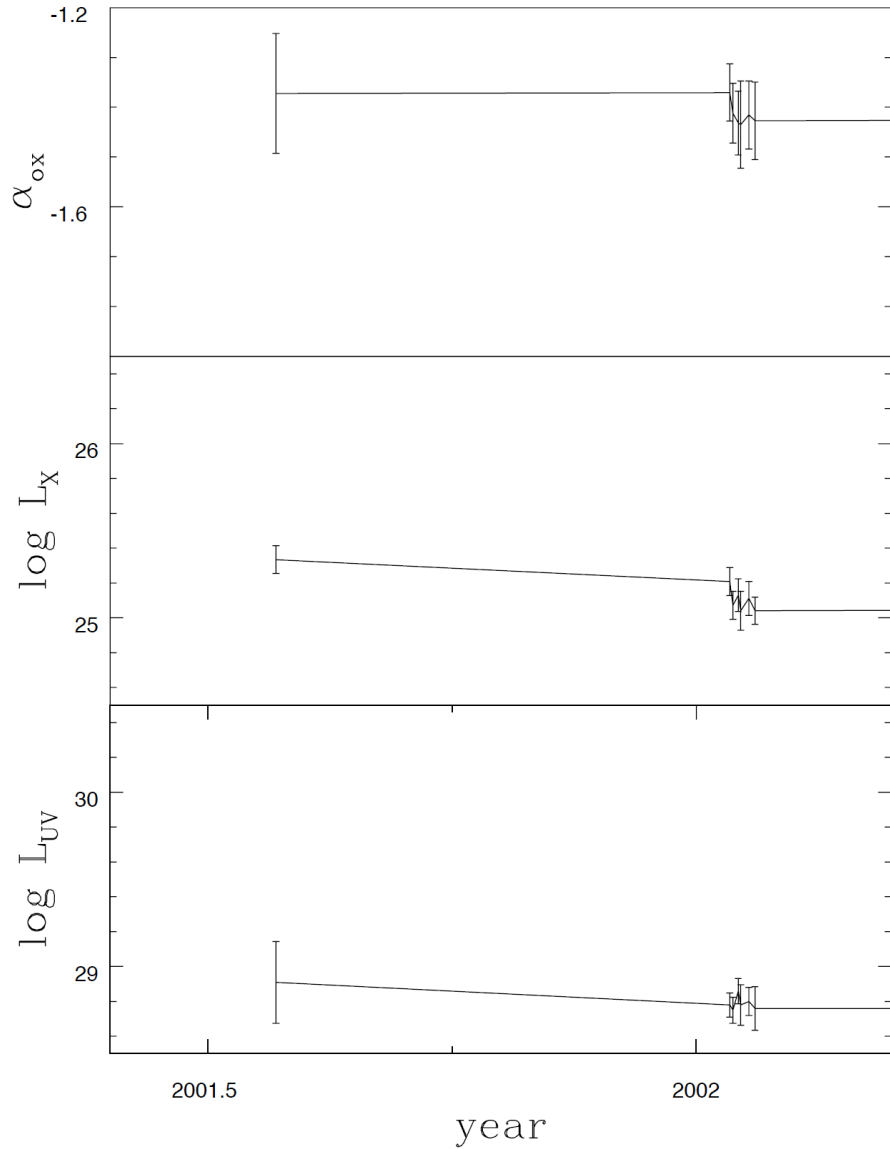
S/N=1.22, $m=22.25\pm0.89$

S/N=3.36, $m=21.79\pm0.58$

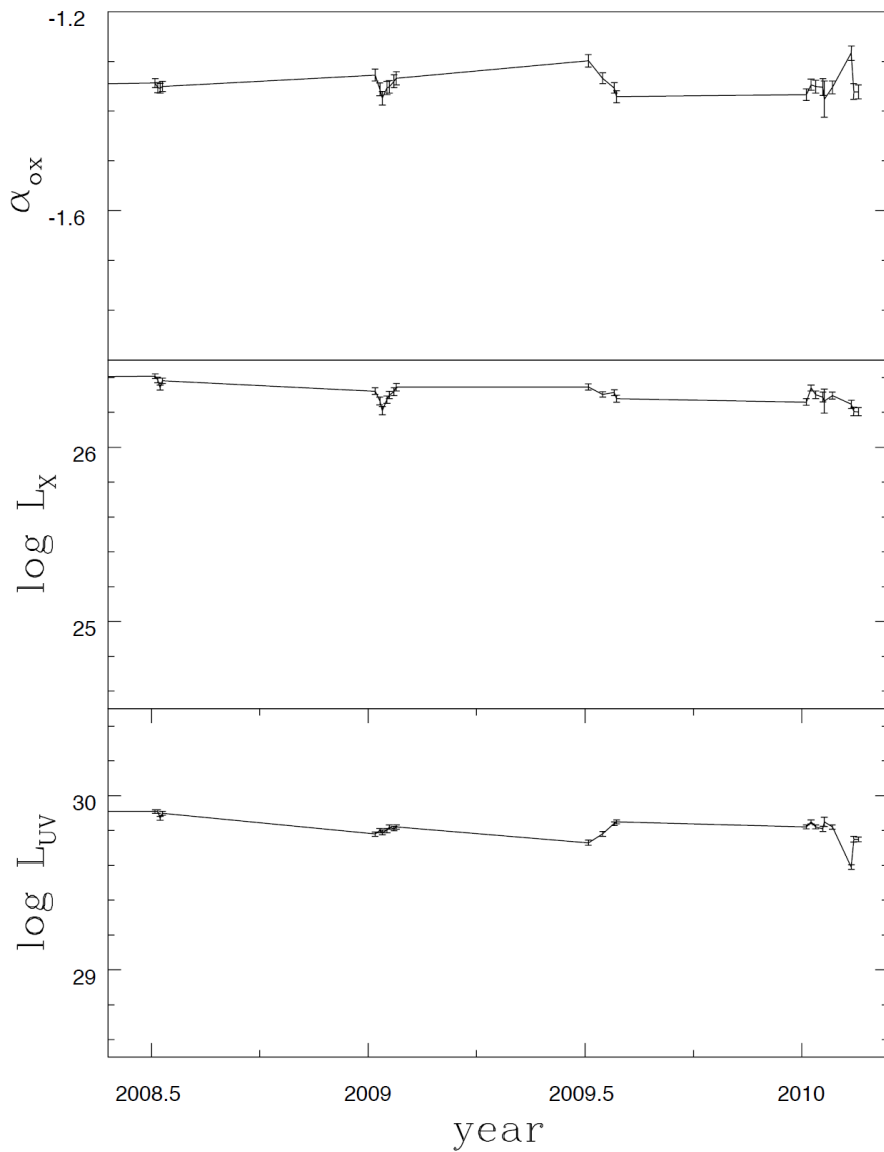
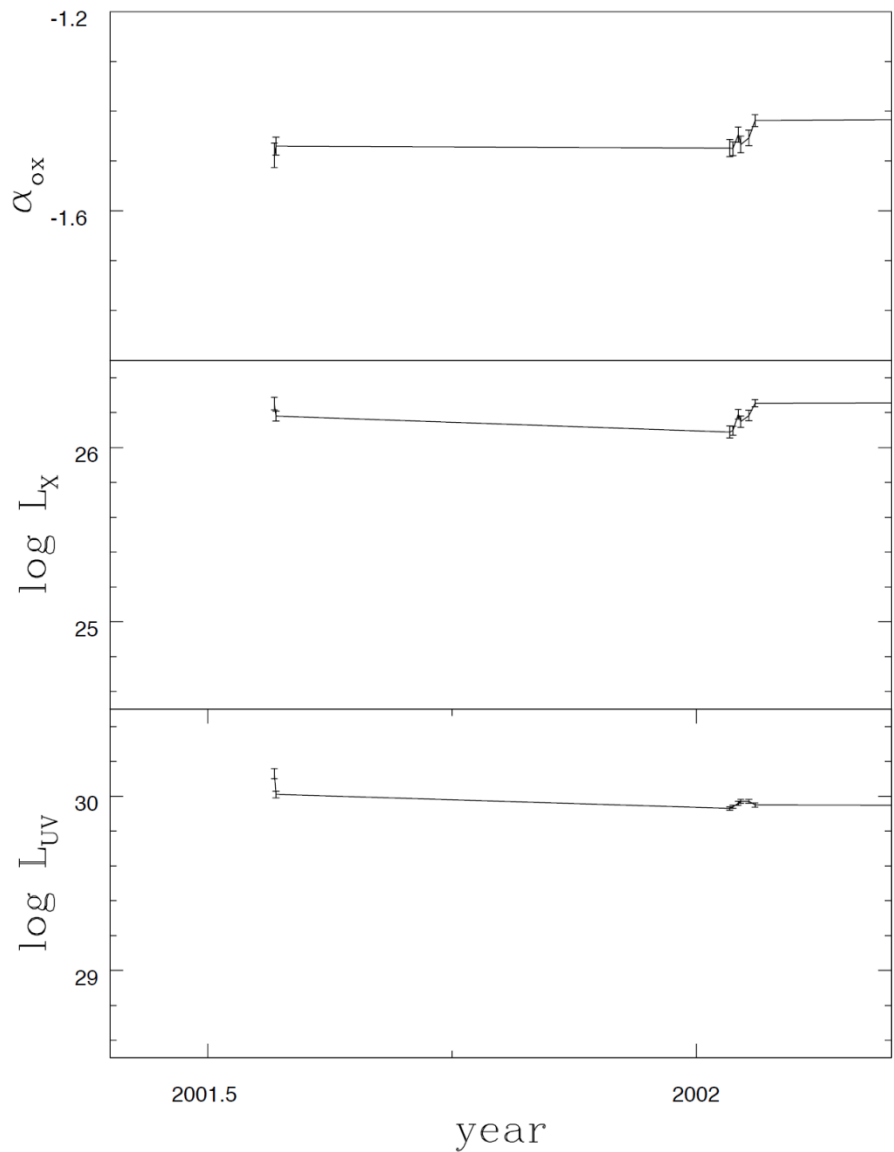
Light-curve (source 203, 33 epochs)



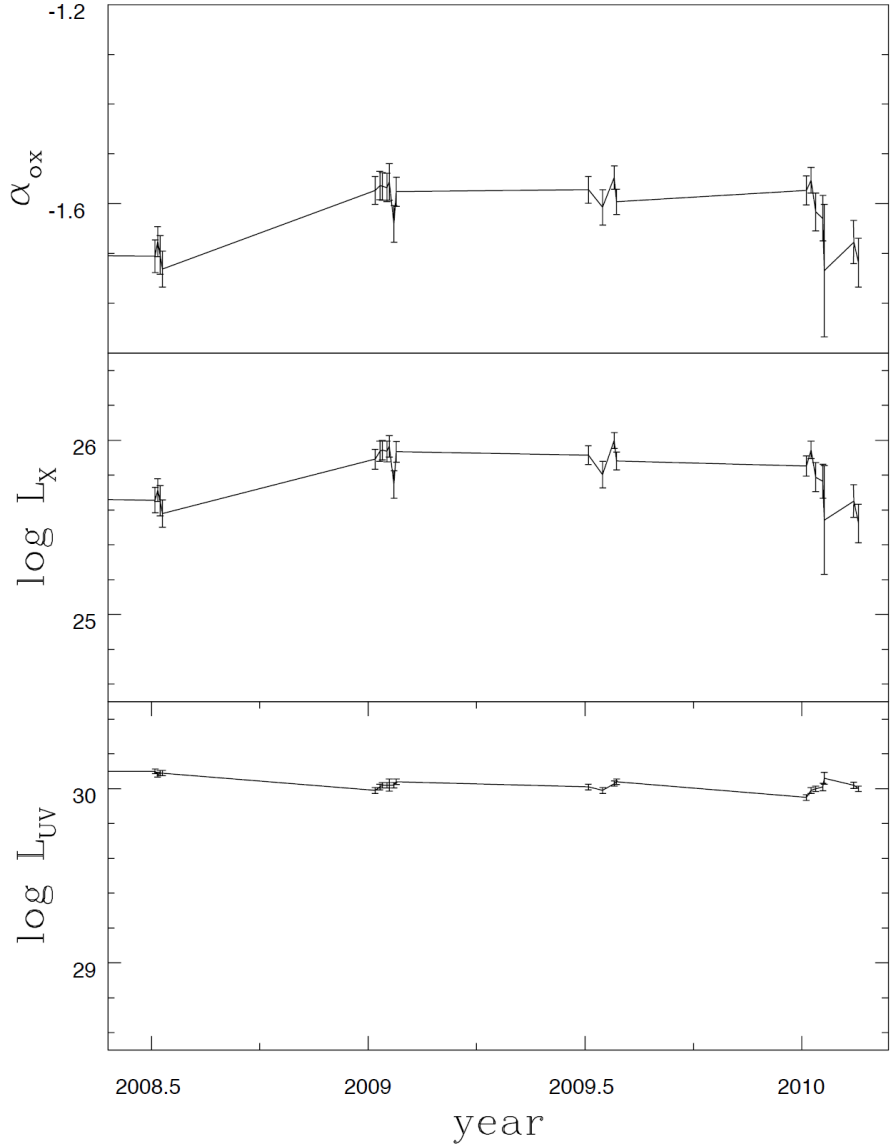
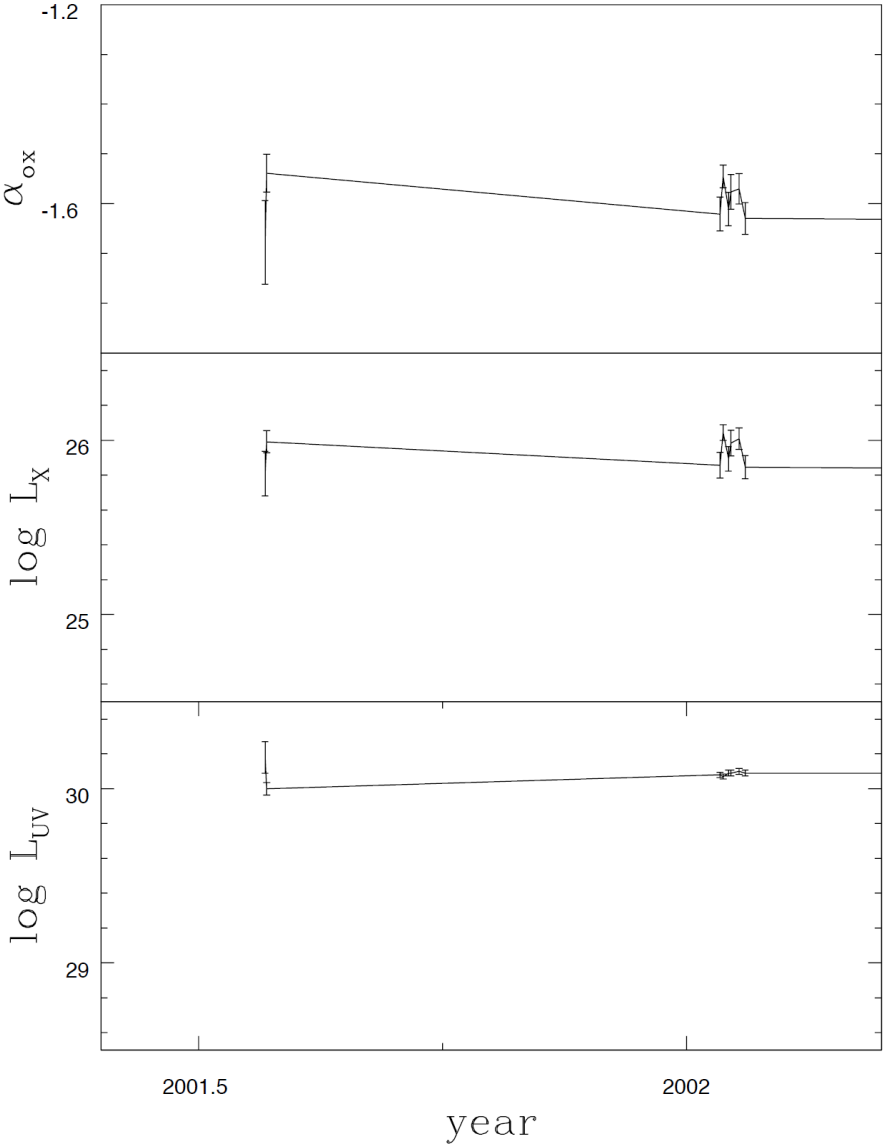
Light-curve (source 289, 30 epochs)



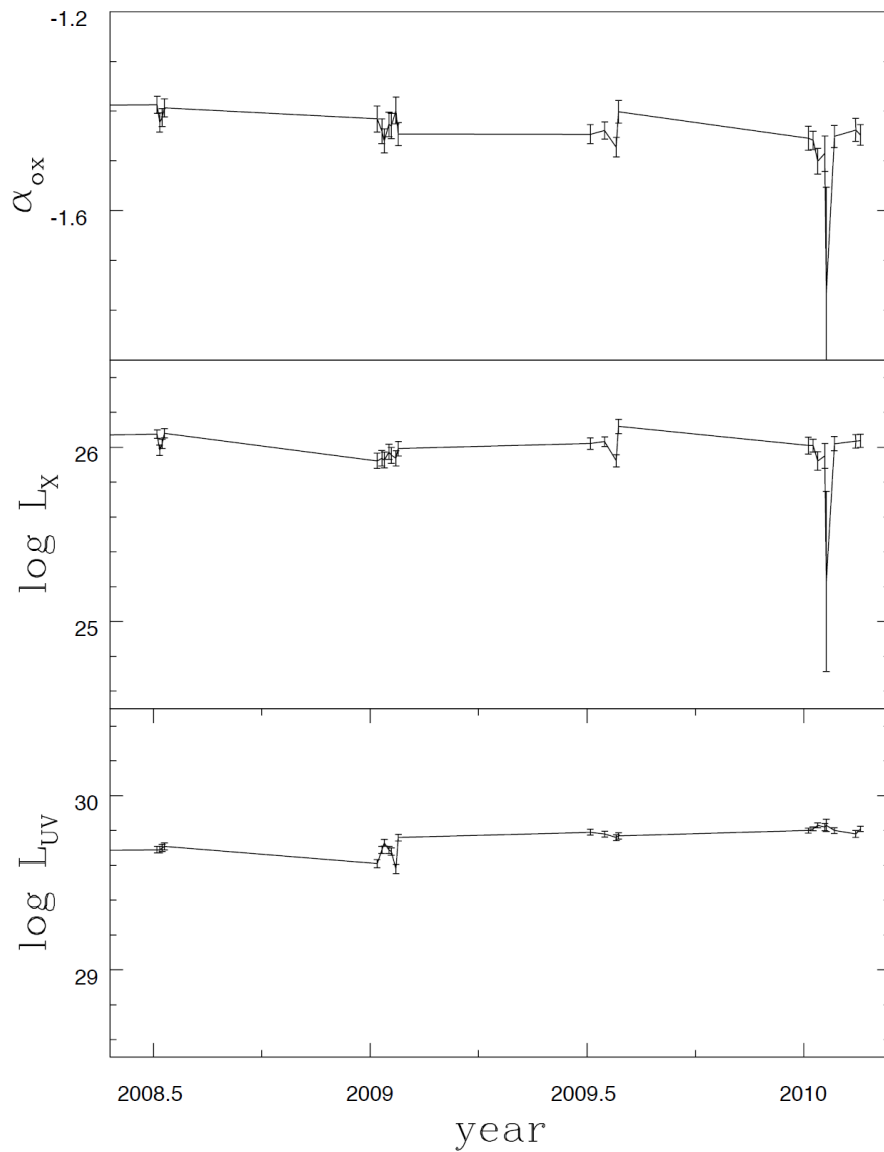
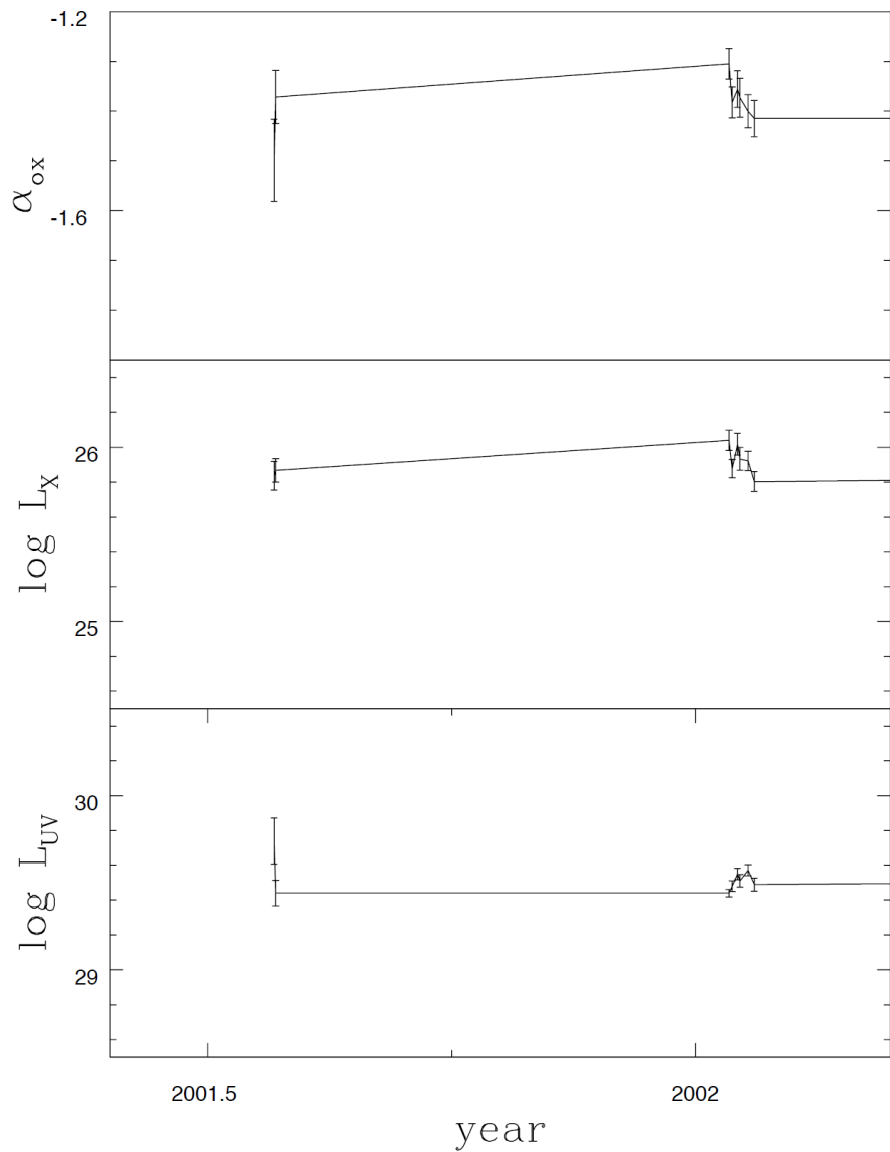
Light-curve (source 319, 32 epochs)



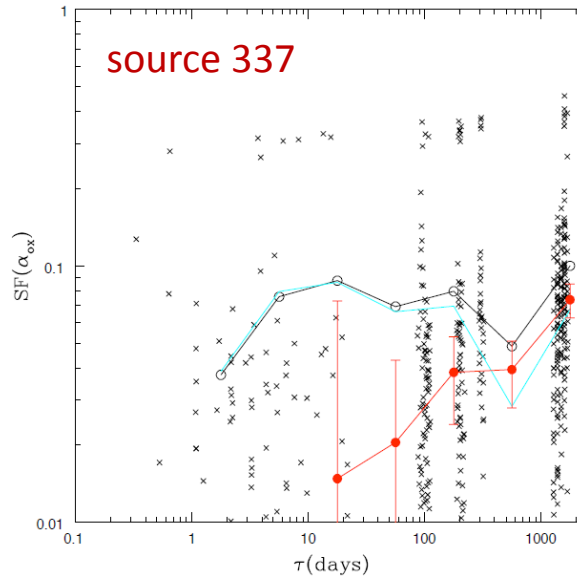
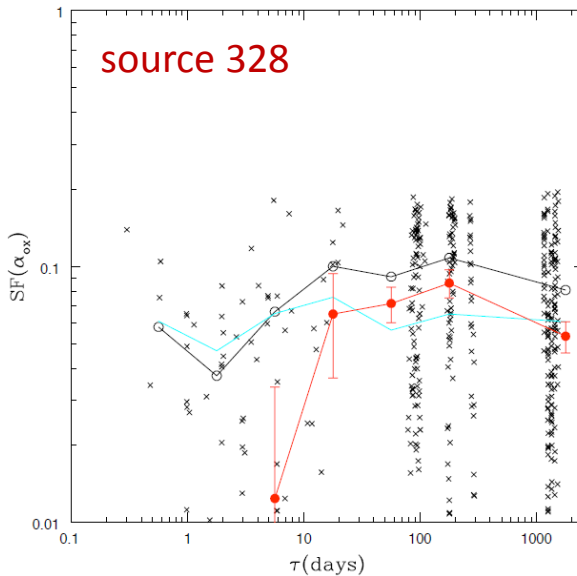
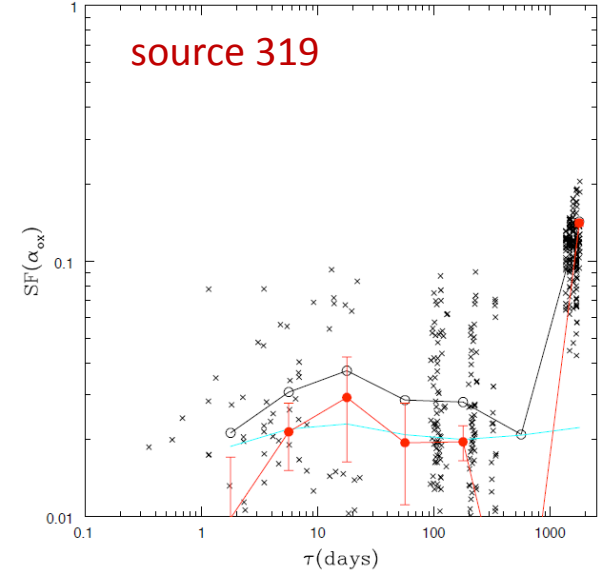
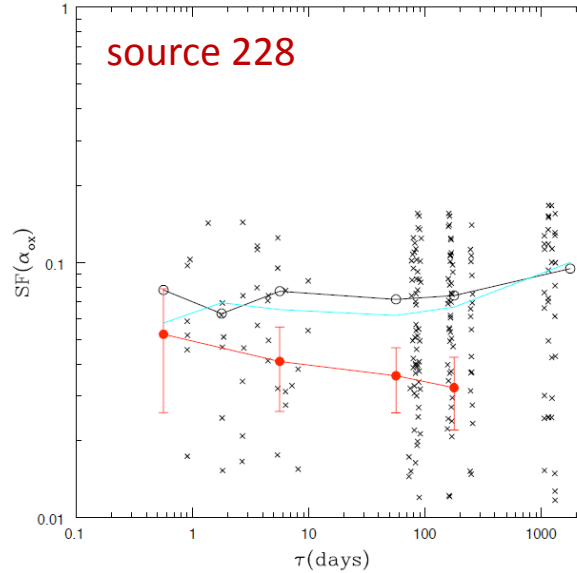
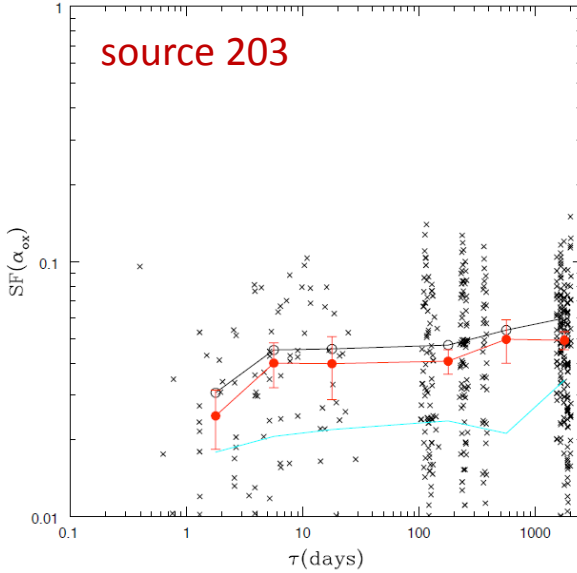
Light-curve (source 328, 30 epochs)



Light-curve (source 337, 31 epochs)



Individual structure functions



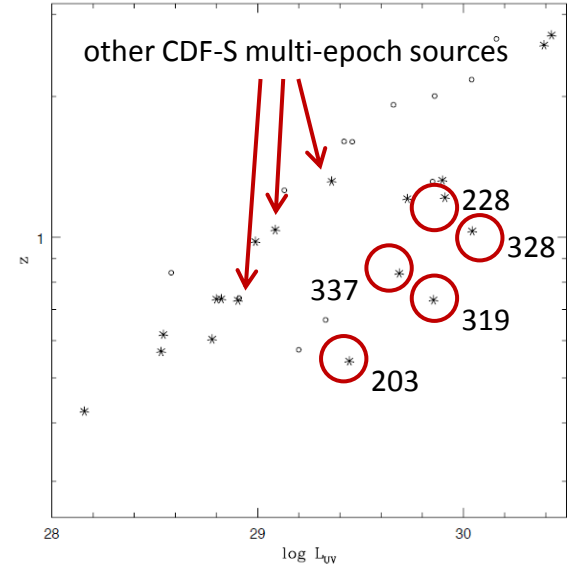
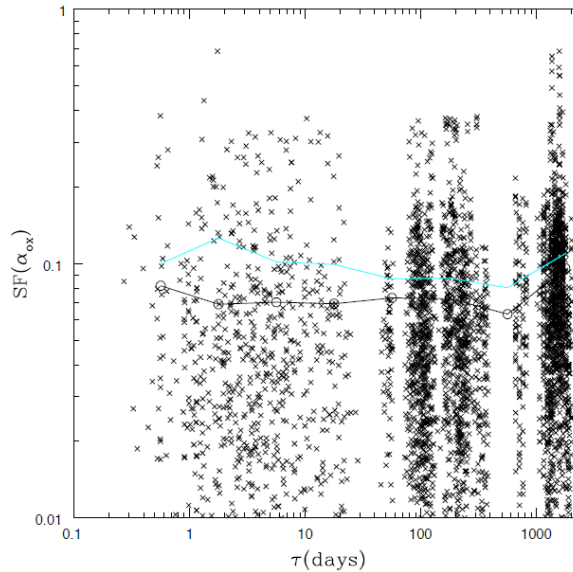
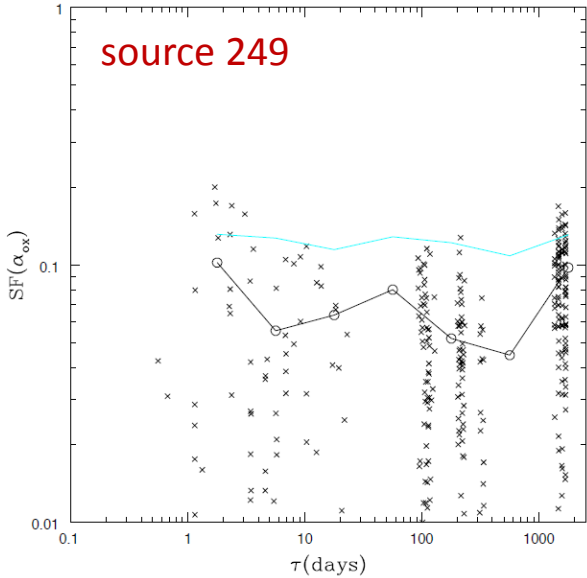
$$SF(\tau) = \sqrt{\frac{\pi}{2}} \langle |\alpha_{ox}(t+\tau) - \alpha_{ox}(t)| \rangle^2 - \sigma_n^2$$

Structure functions of the brighter sources

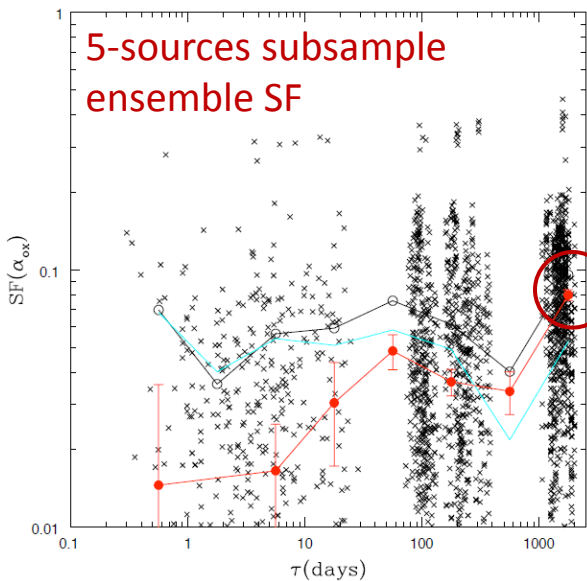
Black lines: uncorrected SFs
Cyan lines: average values of the noise in each bin

Red lines: structure functions of α_{ox} corrected for the photometric noise

Ensemble structure functions



Luminosity-redshift plane



Most of the sources present large photometric noise, greater than the intrinsic variability. The signal emerges only for the brightest sources, while it is completely buried in the ensemble structure function.

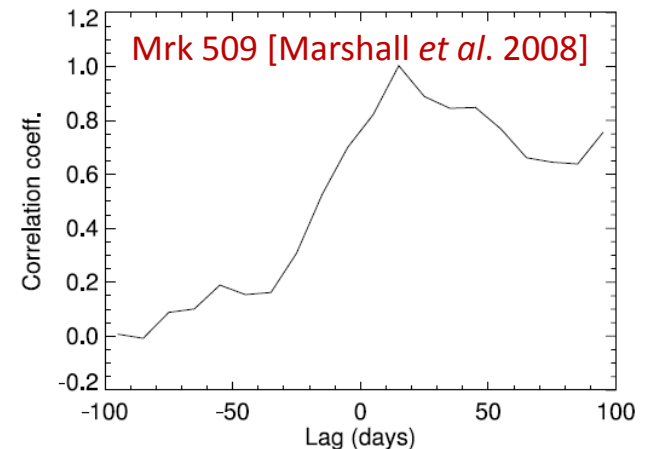
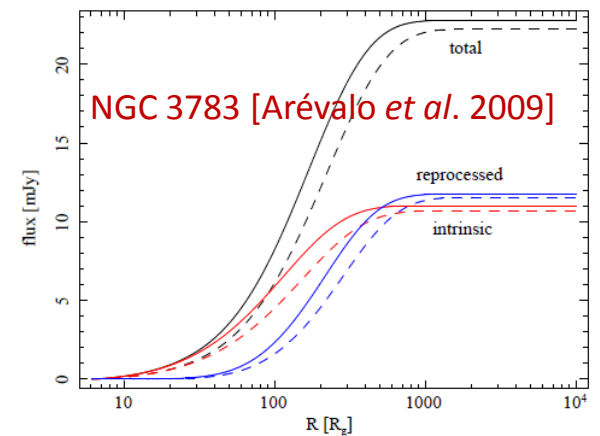
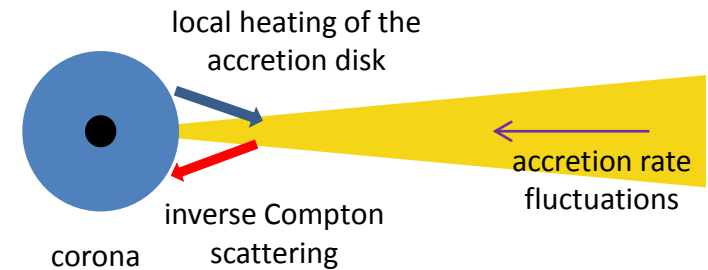
5-sources subsample ensemble SF: it allows to calculate the intra-source dispersion (0.08), that accounts for 50% of the total scatter ($\sigma=0.113$, $\Delta\alpha_{\text{ox}}$ computed with respect to the reference relation from Just *et al.* 2007).

Disk-corona coupling

The broad range of time scales that characterize the variability could derive from fluctuations in the accretion rate, which propagate in the accretion flow, modulating the emission [Lyubarskii 1997, Arévalo 2006]; possibly because of these fluctuations, the optical variability amplitude generally exceeds X-ray variations on long time scales [Arévalo *et al.* 2008, 2009].

Previous studies attempted to correlate X-ray and optical variability considering intense observing campaigns of single objects [Papadakis *et al.* 2000, Maoz *et al.* 2002, Uttley *et al.* 2005, Marshall *et al.* 2008, Arévalo *et al.* 2009], and the results depended on their characteristics:

- many of the relevant time scales (orbital, thermal, viscous) increase linearly with BH mass of the source, determining the lag between X-ray and optical variations [Marshall *et al.* 2008];
- some analyses indicate the X-rays lag the UV [Marshall *et al.* 2008, Doroshenko *et al.* 2009], while other studies find the reverse [Shemmer *et al.* 2001, Arévalo *et al.* 2009].



Conclusions and perspectives

An estimate of the intrinsic α_{ox} variability is obtained from the ensemble structure function of the subsample of brightest sources, corrected for the photometric noise. It strengthens our previous results: intra-source dispersion ($\sigma=0.08$) accounts for 50% of the total variance.

Photometric noise dominates intrinsic variability in the total sample ensemble structure function.

Possible improvements:

- get optimised X-ray fluxes (from the collaboration, in progress);
- compute the optical fluxes increasing S/N ratio (through the interactive photometric analysis of the OM images with SAS).

Next step in the study of the CDF-S sample will be the analysis of the cross-correlation between X-ray and optical/UV variations, trying to determine the delay between the emissions in these spectral bands for the sources with more measurements. The sampling is characterized by sets of 4-10 observations performed during periods of 10-20 days, which could allow to detect possible lags of few days for moderate/high-luminosity sources. It is possible to improve the sampling through the methods of Zu *et al.* (2011), that enable to estimate probabilities within the gaps between consecutive observations.